Nuclear-recoil differential cross sections for the double photoionization of helium

Sh. A. Abdel-Naby and M. S. Pindzola
Department of Physics, Auburn University, Auburn, Alabama 36849, USA

J. Colgan
Theoretical Division, Los Alamos National Laboratory, Los Alamos, New Mexico 87545, USA

(Received 15 May 2012; published 27 July 2012)

The time-dependent close-coupling method for the double photoionization of atoms is extended to compute fully differential nuclear-recoil cross sections. Excellent agreement is found between our calculated double-photoionization total cross sections of He and the measurements at all photon energies. Differential cross-section results are presented for the single-photon double ionization of He at photon energies of 99, 125, and 225 eV. The single-differential cross-section results at 99 eV agree with previous theory and experiment. Symmetric momentum distributions are found in the plane perpendicular to the polarization direction, while dipolelike momentum distributions are found in the other two planes. The variation of the nuclear-recoil triple-differential cross sections of He^{2+} with the nuclear-recoil momenta are presented. The total cross sections for the nuclear-recoil of He^{2+} match the corresponding ones for the double electron ejection of He for all the studied photon energies.

DOI: 10.1103/PhysRevA.86.013424 PACS number(s): 32.80.Fb

I. INTRODUCTION

Recoil-ion momentum spectroscopy (RIMS) has become an indispensable tool in atomic collision experiments in recent years. The advent of cold-target RIMS has led to the measurement of many scattering quantities involving the ionization of small atoms and molecules by photon absorption and charged-particle impact. Usually the first quantity that is measured in such experiments is the distribution of the recoiling ion momentum after the collision. This quantity, which does not require the detection of a scattered electron, has a much larger count rate than multiple coincidence measurements required to measure the angular distribution of the scattered electrons; good statistics can easily be achieved. In single-photon double ionization of He, such measurements were first made in the 1990s [1,2] and were quickly followed by rapid theoretical progress that agreed well with experiment and uncovered further insights into the double-photoionization mechanism [3,4]. Such studies showed how insight may be gleaned into the outgoing electron properties from analysis of the recoil-ion momentum distributions. Since then, the study of the recoil-ion momentum distribution for many double-photoionization processes has been reported. Examples include the recoil-ion distributions for the two-photon double ionization of He [5,6] and for the single-photon double ionization of Li [7].

In this article, we show how the time-dependent close-coupling (TDCC) method for the double photoionization of atoms may be straightforwardly extended to compute recoil-ion momentum distributions. The TDCC approach was first used to study the total cross section for single-photon double ionization of He [8] and then later extended to examine the energy and angle differential cross sections for the single-photon double ionization of He at 20 eV excess energy [9]. Since then the TDCC method has been applied to many double-photoionization events in a variety of small atoms and molecules [10]. We first compare the TDCC nuclear-recoil differential cross sections with previous results [2–4] for the single-photon double ionization of He at 20 eV excess energy. We then present TDCC nuclear-recoil differential cross sections for the double photoionization of He at photon energies of 125 and 225 eV.

The rest of the article is structured as follows: In Sec. II, we briefly review the TDCC method and then present detailed expressions for the electron angle differential and nuclear-recoil differential cross sections; in Sec. III, we present double-photoionization cross-section results for He at photon energies of 99, 125, and 225 eV; and in Sec. IV, we conclude with a brief summary. Unless otherwise stated, we will use atomic units.

II. THEORY

A. Time-dependent close-coupling method

For the double photoionization of He, the time-dependent Schrödinger equation in the weak field limit is given by

$$i\frac{\partial\Psi(\vec{r}_1,\vec{r}_2,t)}{\partial t} = H_{\rm atom}\Psi(\vec{r}_1,\vec{r}_2,t)+H_{\rm rad}\Psi_0(\vec{r}_1,\vec{r}_2)\,e^{-iE_0t}\,, \tag{1}$$

where

$$H_{\rm atom} = \sum_i^2\left(-\frac{1}{2}\nabla_i^2-\frac{Z}{r_i}\right)+\frac{1}{|\vec{r}_1-\vec{r}_2|} \tag{2}$$

and $Z = 2$ for He. For a linearly polarized radiation field in the length gauge,

$$H_{\rm rad} = A(t)\cos\omega t\sum_i^2(r_i\cos\theta_i), \tag{3}$$

where ω is the radiation field frequency and $A(t)$ is the radiation field amplitude.

The time-dependent close-coupling equations for the ground-state wave function $\Psi_0(\vec{r}_1,\vec{r}_2)$ and ground-state energy E_0 are given by [10]

$$-\frac{\partial\bar{P}^{L_0S}_{l_1l_2}(r_1,r_2,\tau)}{\partial\tau} = T_{l_1l_2}(r_1,r_2)\bar{P}^{L_0S}_{l_1l_2}(r_1,r_2,\tau) + \sum_{l_1',l_2'}V^{L_0}_{l_1l_2,l_1'l_2'}(r_1,r_2)\bar{P}^{L_0S}_{l_1'l_2'}(r_1,r_2,\tau). \tag{4}$$

The time evolution of the radial wave function $\bar{P}^{L_0S}_{l_1l_2}(r_1,r_2,\tau)$ in imaginary time τ is governed by the one-body kinetic and nuclear interaction operator $T_{l_1l_2}(r_1,r_2)$ and the two-body electrostatic repulsion operator $V^{L_0}_{l_1l_2,l_1'l_2'}(r_1,r_2)$.

The time-dependent close-coupling equations for the total wave function $\Psi(\vec{r}_1,\vec{r}_2,t)$ are given by [10]

$$\begin{aligned} i\frac{\partial P^{LS}_{l_1l_2}(r_1,r_2,t)}{\partial t} &= T_{l_1l_2}(r_1,r_2)P^{LS}_{l_1l_2}(r_1,r_2,t) \\ &+ \sum_{l_1',l_2'} V^{L}_{l_1l_2,l_1'l_2'}(r_1,r_2)P^{LS}_{l_1'l_2'}(r_1,r_2,t) \\ &+ \sum_{l_1',l_2'} W^{LL_0}_{l_1l_2,l_1'l_2'}(r_1,r_2,t)\bar{P}^{L_0S}_{l_1'l_2'}(r_1,r_2,\tau\to\infty)e^{-iE_0t}. \end{aligned} \quad (5)$$

The time evolution of the radial wave function $P^{LS}_{l_1l_2}(r_1,r_2,t)$ in real time t is governed by the one-body kinetic and nuclear interaction operator $T_{l_1l_2}(r_1,r_2)$, the two-body electrostatic repulsion operator $V^{L}_{l_1l_2,l_1'l_2'}(r_1,r_2)$, and the one-body radiation field operator $W^{LL_0}_{l_1l_2,l_1'l_2'}(r_1,r_2,t)$.

B. Differential cross sections

For double photoionization of He, the conservation of energy is given by

$$\omega - I_p = E_1 + E_2, \quad (6)$$

where $I_p = 79.01$ eV is the double-ionization potential and $E_1 = \frac{k_1^2}{2}$ and $E_2 = \frac{k_2^2}{2}$ are the energies of the two outgoing electrons.

1. Electron angle differential cross section

The electron angle differential cross section is given by [10]

$$\frac{d\sigma}{d\alpha d\Omega_1 d\Omega_2} = \frac{\omega}{I}\frac{\partial}{\partial t}\int_0^\infty dk_1\int_0^\infty dk_2\,\delta\left(\alpha-\tan^{-1}\left(\frac{k_2}{k_1}\right)\right) \times |S(k_1,k_2,\Omega_1,\Omega_2,t)|^2, \quad (7)$$

where

$$S(k_1,k_2,\Omega_1,\Omega_2,t) = \sum_{l_1,l_2}(-i)^{l_1+l_2}e^{i(\delta_{l_1}+\delta_{l_2})}P^{LS}_{l_1l_2}(k_1,k_2,t)Y^{L}_{l_1l_2}(\Omega_1,\Omega_2), \quad (8)$$

$$P^{LS}_{l_1l_2}(k_1,k_2,t) = \int_0^\infty dr_1\int_0^\infty dr_2 P_{k_1l_1}(r_1)P_{k_2l_2}(r_2)P^{LS}_{l_1l_2}(r_1,r_2,t), \quad (9)$$

α is a hyperspherical angle in the (k_1,k_2) plane, I is the radiation field intensity, and $Y^{L}_{l_1l_2}(\Omega_1,\Omega_2)$ is a coupled spherical harmonic. The continuum radial orbitals $P_{kl}(r)$ are obtained by direct numerical integration of the time-independent Schrödinger equation for He^+ using standard box normalization with a Coulomb phase shift δ_l. We note that

$$\frac{d\sigma}{dE_1 d\Omega_1 d\Omega_2} = \frac{1}{k_1k_2}\frac{d\sigma}{d\alpha d\Omega_1 d\Omega_2} \quad (10)$$

and

$$\sigma = \int dE_1\int d\Omega_1\int d\Omega_2\,\frac{d\sigma}{dE_1 d\Omega_1 d\Omega_2}. \quad (11)$$

2. Nuclear-recoil differential cross section

The nuclear-recoil differential cross section is given by

$$\frac{d\sigma}{d\alpha d\phi_2' dQ_x dQ_y dQ_z} = \frac{\omega}{IQ}\frac{\partial}{\partial t}\int_0^\infty\frac{dk_1}{k_1}\int_0^\infty\frac{dk_2}{k_2}\delta\left(\alpha-\tan^{-1}\left(\frac{k_2}{k_1}\right)\right) \times |S(k_1,k_2,\Omega_1',\Omega_2',t)|^2. \quad (12)$$

The scattering angles for the two outgoing electrons are given by [6]

$$\cos(\theta_1) = \left(Q^2+k_1^2-k_2^2\right)/(2Qk_1), \quad (13)$$

$$\cos(\theta_2) = \left(Q^2+k_2^2-k_1^2\right)/(2Qk_2), \quad (14)$$

and

$$\phi_1 = \phi_2 + \pi, \quad (15)$$

where the magnitude of the nuclear-recoil is given by

$$Q = \sqrt{\left(Q_x^2+Q_y^2+Q_z^2\right)}. \quad (16)$$

The maximum value of Q is $2\sqrt{E}$, where $E = E_1 + E_2$. The angles $(\theta_1,\phi_1,\theta_2,\phi_2)$ are then transformed to angles $(\theta_1',\phi_1',\theta_2',\phi_2')$ with respect to a coordinate frame with the radiation polarization along the z axis. We note that

$$\frac{d\sigma}{dE_1 d\phi_2' dQ_x dQ_y dQ_z} = \frac{1}{k_1k_2}\frac{d\sigma}{d\alpha d\phi_2' dQ_x dQ_y dQ_z}, \quad (17)$$

$$\frac{d\sigma}{dQ_x dQ_y dQ_z} = \int dE_1\int d\phi_2'\,\frac{d\sigma}{dE_1 d\phi_2' dQ_x dQ_y dQ_z}, \quad (18)$$

and

$$\sigma = \int dQ_x\int dQ_y\int dQ_z\,\frac{d\sigma}{dQ_x dQ_y dQ_z}. \quad (19)$$

III. RESULTS

We have carried out calculations for the nuclear-recoil cross sections for the double photoionization of He at photon energies 99, 125, and 225 eV. The initial ground state $\Psi_0^{^1S}(\vec{r}_1,\vec{r}_2,t)$ of the He atom is obtained by an expansion in coupled spherical harmonics and subsequent relaxation of the time-dependent Schrödinger equation in imaginary time $\tau = it$ [see Eq. (4)] [10]. Four coupled channels are sufficient for convergence in the case of photon energies 99 and 125 eV ($l_1,l_2 \leqslant 3$), while nine coupled channels are required for the photon energy 225 eV ($l_1,l_2 \leqslant 9$). About 500 imaginary time steps with $\Delta\tau = 0.01$ are needed for convergence for the case of 99 and 125 eV (6000 imaginary time steps with $\Delta\tau = 0.001$ for the case of photon energy 225 eV) on a uniform 768×768 lattice with a mesh spacing of $\Delta r = 0.1$. The ground-state energy is found to be $E_0 = 78.15$ eV for the photon energies 99 and 125 eV ($E_0 = 78.16$ eV for the photon energy 225 eV), which are close to the exact ground-state energy of 79.01 eV [11]. The electric field is ramped on smoothly over

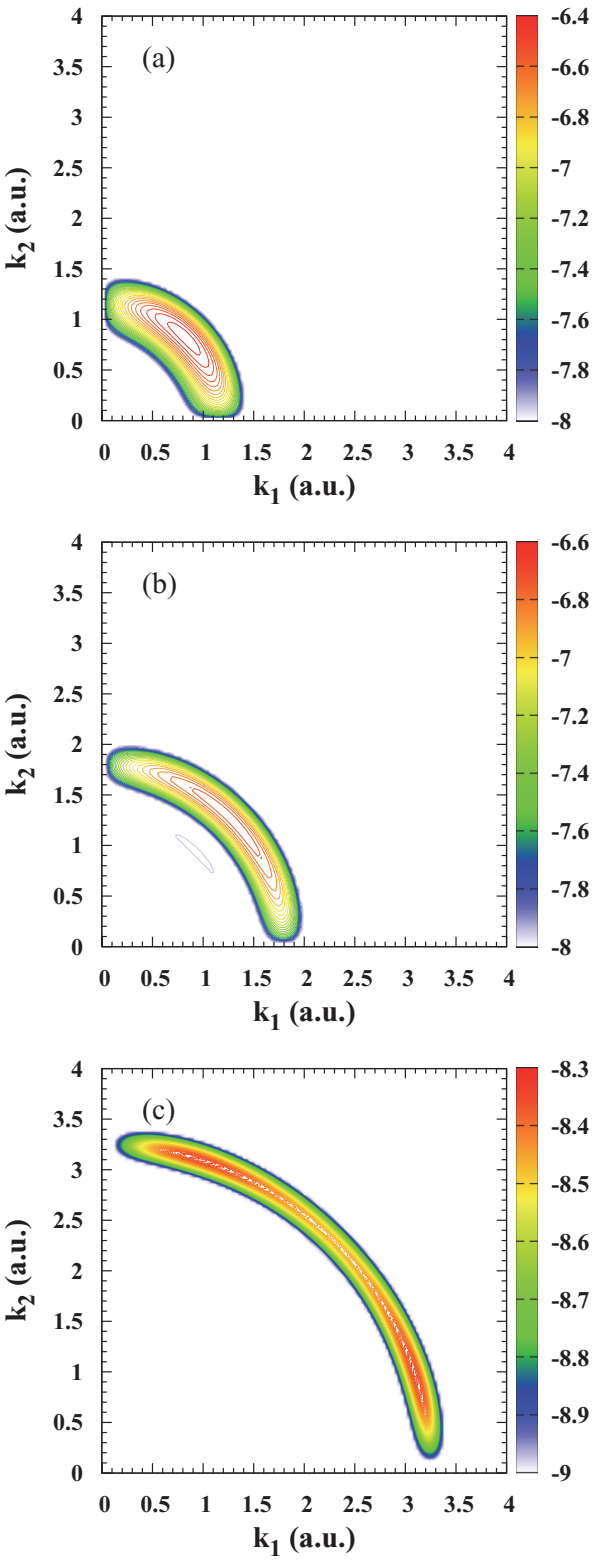

FIG. 1. (Color online) Contour plots of the total double-photoionization probability $\sum_{l_1,l_2} |P^{^1P}_{l_1,l_2}(k_1,k_2,t)|^2$ of He at photon energies of (a) 99 eV, (b) 125 eV, and (c) 225 eV, respectively. The numbers beside the color box are powers of 10.

one-quarter of a field period so that $E(t) = t/T$ for $t < T/4$ and $E(t) = 1$ for $t > T/4$. The final state $\Psi^{^1P}(\vec{r}_1,\vec{r}_2,t)$ is

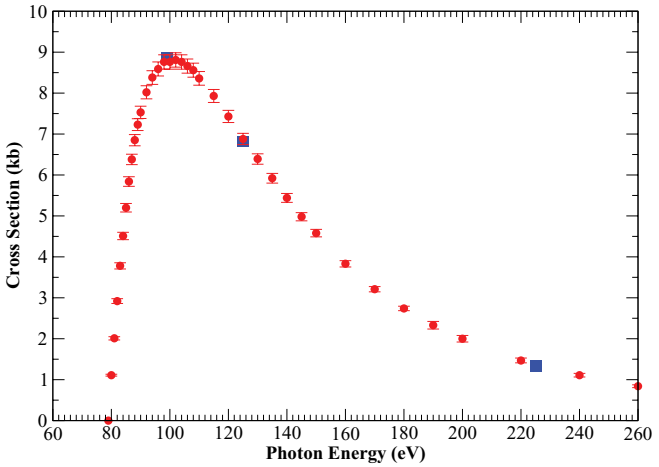

FIG. 2. (Color online) Double-photoionization cross sections of He: solid squares, our TDCC results; solid circles, experimental measurements of Samson *et al*. [13] (1.0 kb = 1.0×10^{-21} cm^2).

obtained by an expansion in coupled spherical harmonics with 8 coupled channels for photon energies 99 and 125 eV ($l_1,l_2 \leqslant 4$) and 18 coupled channels for the photon energy 225 eV ($l_1,l_2 \leqslant 9$). The time-dependent close-coupled equations are solved on the same uniform numerical lattice of 768 × 768 with a mesh spacing of $\Delta r = 0.1$ and time propagated for 10 radiation field periods ($2\pi/\omega$) [see Eq. (5)].

In Fig. 1, we present the total probability density for the double photoionization of He in momentum space k_1 and k_2 at the above three photon energies. The probability densities are characterized by quarters of spherical shells, with the maximum densities located at radii of 1.24, 1.86, and 3.29 a.u. for the photon energies 99, 125, and 225 eV, respectively. The positions of the maximum probability densities satisfy the relation $\Delta E = k_1^2/2 + k_2^2/2$, where ΔE is the excess photon energy as given by Eq. (6) and the other two terms give the kinetic energies for the two photoionized electrons of He. The peak of the total probability of the double photoionization of He in momentum space is located along a straight line defined by the equation $k_2 = k_1$, or at a hyperspherical angle $\alpha = 45^\circ$ ($\tan\ \alpha = k_2/k_1$) for the photon energies 99 and 125 eV. On the other hand, two distinct peaks can be recognized at two hyperspherical angles $\alpha = 20^\circ$ and 70° for the photon energy of 225 eV. This reflects the more U-shaped nature of the electron energy distribution function [12]. As the photon energy increases, the total probability density of the double photoionization of He decreases. In Fig. 2, we compare our calculated total integral double-photoionization cross sections of He, using Eq. (11), with the experimental results of Samson *et al*. [13], where excellent agreement is obtained at the three photon energies. The reduction in the probability densities found in Fig. 1 as the photon energy increases is reflected in the double-photoionization cross section of He.

In Fig. 3, we present contour plots of the nuclear-recoil triple-differential cross section (TDCS) of He^{2+} in the x-y plane using Eq. (18) and setting $Q_z = 0$ at the three photon energies of 99, 125, and 225 eV, where the electric field is polarized in the z direction. As we can see, the nuclear-recoil TDCS of He^{2+} is symmetric in the x-y plane, which is perpendicular to the polarization direction. On the other hand,

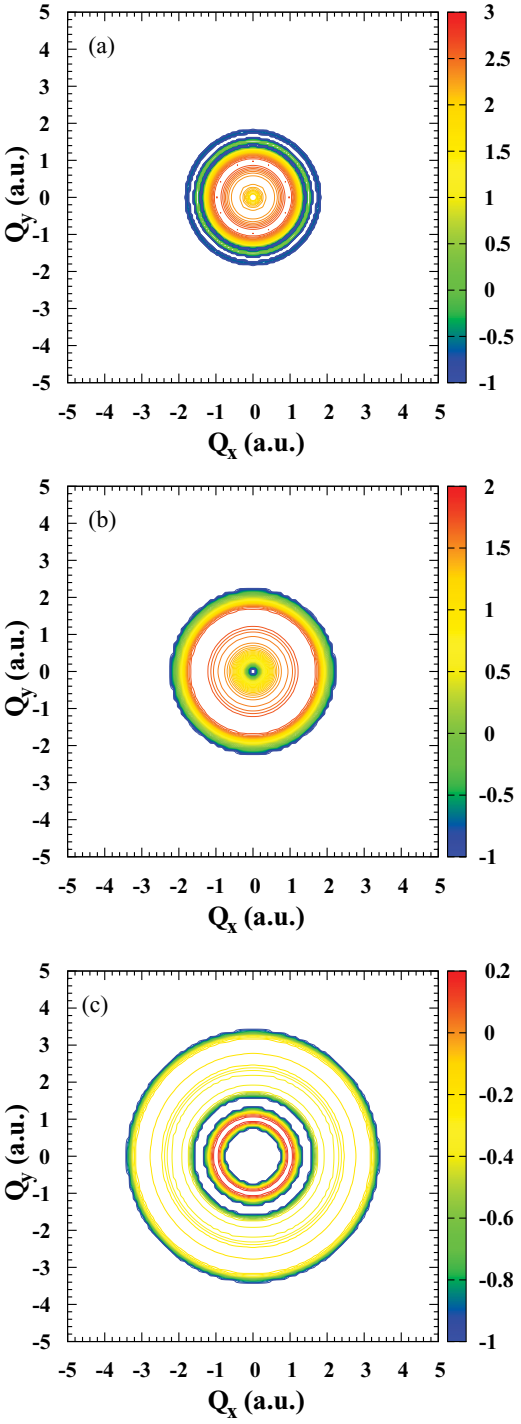

FIG. 3. (Color online) Nuclear-recoil triple-differential cross section of He^{2+} in the x-y plane (setting $Q_z = 0$) at photon energies (a) 99 eV, (b) 125 eV, and (c) 225 eV, respectively. The numbers beside the color box are powers of 10.

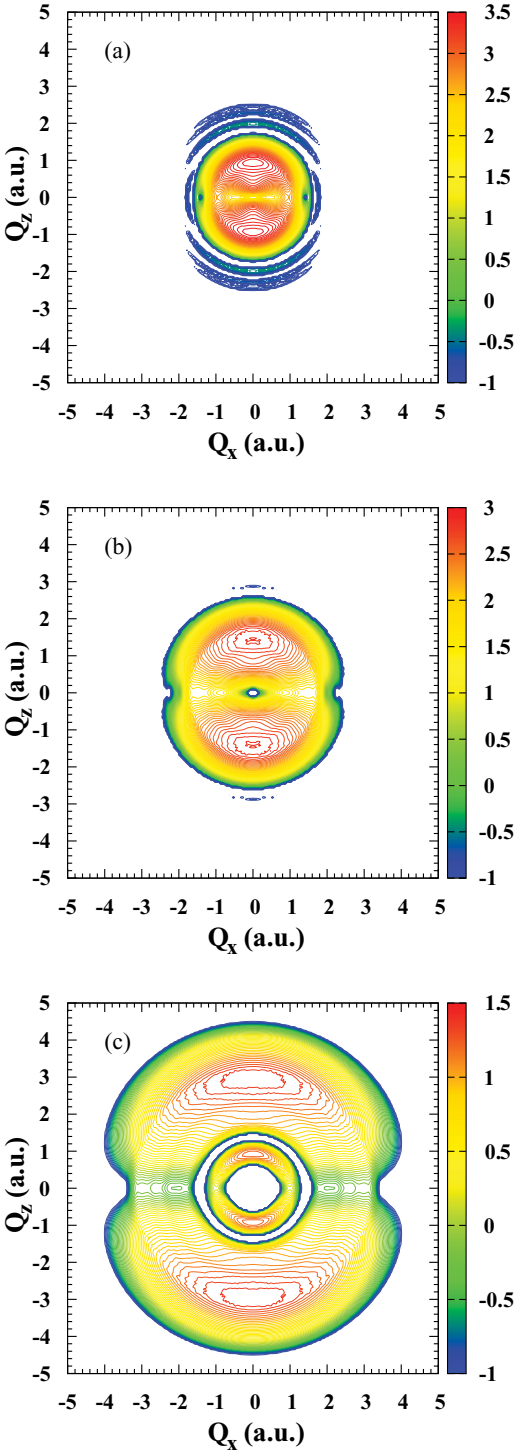

FIG. 4. (Color online) Nuclear-recoil triple-differential cross section of He^{2+} in the x-z plane (setting $Q_y = 0$) at photon energies (a) 99 eV, (b) 125 eV, and (c) 225 eV, respectively. The numbers beside the color box are powers of 10.

if we use Eq. (18) and set $Q_y = 0$, the nuclear-recoil TDCS of He^{2+} shows a dipolelike distribution in the x-z plane, as shown in Fig. 4. Similar features are observed when we examine the nuclear-recoil TDCS of He^{2+} in the y-z plane, where we set $Q_x = 0$. So, the nuclear-recoil momentum distributions are symmetric in the plane perpendicular to the polarization direction, while dipolelike distributions are seen in the other two planes. These distributions were experimentally seen at lower photon energies [1], where the electric field was polarized in the z direction, and at a photon energy of 99 eV [2], where the electric field was polarized in the x direction.

The magnitudes of the nuclear-recoil TDCS of He^{2+} as a function of the nuclear momenta Q_x, Q_y, and Q_z at the

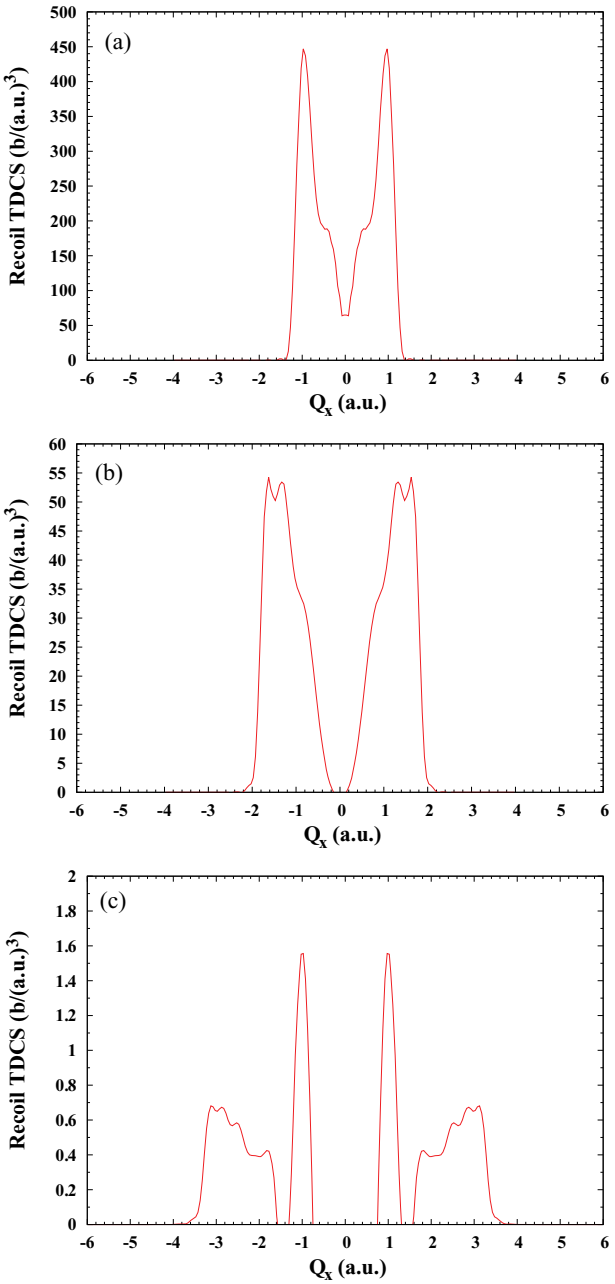

FIG. 5. (Color online) The variation of the TDCS of He^{2+} as a function of the nuclear-recoil momentum in the x direction with $Q_y = Q_z = 0$ at photon energies (a) 99 eV, (b) 125 eV, and (c) 225 eV, respectively. The TDCS are given in units of barns per momentum in atomic units cubed [b/(a.u.)^3] (1.0 b = 1.0×10^{-24} cm^2 and 1.0 a.u. = 1.99×10^{-19} g cm/s).

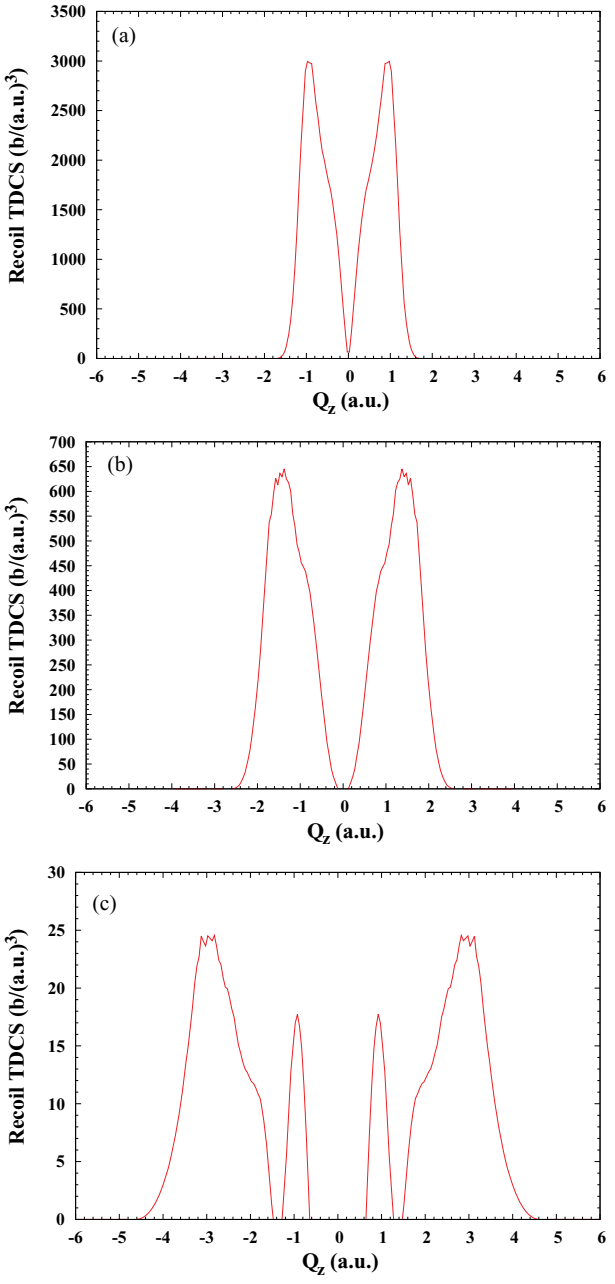

FIG. 6. (Color online) The variation of the TDCS of He^{2+} as a function of the nuclear-recoil momentum in the z direction with $Q_x = Q_y = 0$ at photon energies (a) 99 eV, (b) 125 eV, and (c) 225 eV, respectively. The TDCS's are given in units of barns per momentum in atomic units cubed [b/(a.u.)^3] (1.0 b = 1.0×10^{-24} cm^2 and 1.0 a.u. = 1.99×10^{-19} g cm/s).

above three photon energies can be calculated using Eq. (18). The variation of the nuclear-recoil TDCS of He^{2+} with Q_x, setting $Q_y = Q_z = 0$, for all three photon energies is shown in Fig. 5, while its variation with Q_z (setting $Q_x = Q_y = 0$) is shown in Fig. 6. The study of the variation of the nuclear-recoil TDCS of He^{2+} with Q_y matches exactly its variation with Q_x. The nuclear-recoil TDCS's are given in units of barns per nuclear momenta in atomic units cubed [b/(a.u.)^3] (1.0 b = 1.0×10^{-24} cm^2 and 1.0 a.u. = 1.99×10^{-19} g cm/s). As the photon energy increases, the maximum limits of the nuclear momenta increase too. The momentum distributions in the z direction are broader than the corresponding ones in the x direction for all three photon energies, which shows that the He^{2+} ion accelerates more in the polarization direction. The spread of the nuclear-recoil momenta is governed by Eq. (16), with the total nuclear-recoil momentum given by $\vec{Q} = -(\vec{k}_1 + \vec{k}_2)$, where the values of Q vary between $Q = \pm(|k_1| \pm |k_2|)$. The magnitudes of the nuclear-recoil TDCS of He^{2+} in the z directions are higher by factors of 6, 12, and 11 than those in

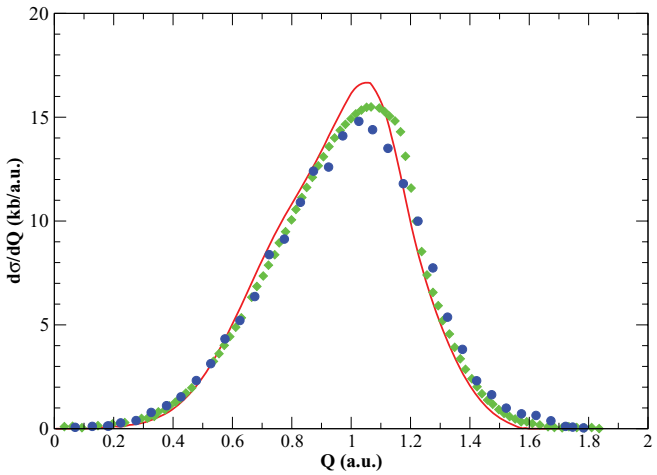

FIG. 7. (Color online) Nuclear-recoil single-differential cross section $d\sigma/dQ$ of He^{2+} as a function of the recoil momentum Q at a photon energy of 99 eV ($\vec{Q} = \vec{k}_1 + \vec{k}_2$). Red solid line is the present calculations; blue circles are measured values [1]; green diamonds are calculated data [4] (1.0 kb $= 1.0 \times 10^{-21}$ cm^2 and 1.0 a.u. $= 1.99 \times 10^{-19}$ g cm/s).

the x direction for the photon energies of 99, 125, and 225 eV, respectively.

A comparison between our results for the nuclear-recoil single-differential cross section (SDCS) $d\sigma/dQ$ of He^{2+} as a function of the nuclear momentum Q at a photon energy of 99 eV with calculated [4] and measured values [1] is shown in Fig. 7. The single-differential cross section is found by transforming the differential cross section of Eq. (18) to spherical polar coordinates and integrating over the polar angles. The maximum value of $Q = 2\sqrt{(E)} = 1.75$ a.u., where $E = 20$ eV is the excess energy. Very good agreement is found between our results and the experimental values [1], with differences varying between 8% and 13% at higher values of Q and at the peak of the nuclear-recoil SDCS, respectively. Our results confirm the asymmetric distribution predicted by the experimental measurements [1].

The total nuclear-recoil cross sections for He^{2+}, using Eq. (19), are found to be 8.78, 6.77, and 1.34 kb for the photon energies of 99, 125, and 225 eV, respectively (1.0 kb $= 1.0 \times 10^{-21}$ cm^2). These values exactly match the corresponding ones for the double electron ejection of He using Eq. (11), which confirms our theoretical representation for the nuclear-recoil problem.

IV. SUMMARY

We have carried out calculations for the nuclear-recoil TDCS of He^{2+} at photon energies of 99, 125, and 225 eV, respectively. In momentum space, the maximum probability densities for the double photoionization of He are located at radii governed by the excess energy relation. Excellent agreement is found between our calculated total double-photoionization cross section of He and the measurements at all photon energies. Symmetric momentum distributions are found in the plane perpendicular to the polarization direction, while dipole-like momentum distributions are found in the other two planes, where the polarization in the z direction exists for all the above photon energies. The variations of the nuclear-recoil TDCS of He^{2+} with the recoil momenta Q_x, Q_y are exactly the same, while higher values are found in the case of Q_z. The single-differential cross-section results at 99 eV agree with previous theory and experiment. The total cross sections for the nuclear-recoil of He^{2+} match the corresponding ones for the double electron ejection of He for the studied photon energies, which confirms that the TDCC method is successfully extended to compute the nuclear-recoil momentum distributions of He^{2+}.

ACKNOWLEDGMENTS

This work was supported in part by grants from the US Department of Energy and the US National Science Foundation. The Los Alamos National Laboratory is operated by Los Alamos National Security, LLC for the NNSA of the US DOE under contract No. DE-AC206NA25396. Computational work was carried out at the National Energy Research Scientific Computing Center in Oakland, California, and the National Institute for Computational Sciences in Knoxville, Tennessee.

[1] R. Dörner, J. M. Feagin, C. L. Cocke, H. Bräuning, O. Jagutzki, M. Jung, E. P. Kanter, H. Khemliche, S. Kravis, V. Mergel, M. H. Prior, H. Schmidt-Böcking, L. Spielberger, J. Ullrich, M. Unversagt, and T. Vogt, Phys. Rev. Lett. **77**, 1024 (1996).

[2] R. Dörner, H. Bräuning, J. M. Feagin, V. Mergel, O. Jagutzki, L. Spielberger, T. Vogt, H. Khemliche, M. H. Prior, J. Ullrich, C. L. Cocke, and H. Schmidt-Böcking, Phys. Rev. A **57**, 1074 (1998).

[3] J. M. Feagin, J. Phys. B **29**, L551 (1996).

[4] M. Pont and R. Shakeshaft, Phys. Rev. A **54**, 1448 (1996).

[5] A. Rudenko, L. Foucar, M. Kurka, T. Ergler, K. U. Kühnel, Y. H. Jiang, A. Voitkiv, B. Najjari, A. Kheifets, S. Lüdemann, T. Havermeier, M. Smolarski, S. Schössler, K. Cole, M. Schöffler, R. Dörner, S. Düsterer, W. Li, B. Keitel, R. Treusch, M. Gensch, C. D. Schröter, R. Moshammer, and J. Ullrich, Phys. Rev. Lett. **101**, 073003 (2008).

[6] D. A. Horner, C. W. McCurdy, and T. N. Rescigno, Phys. Rev. A **78**, 043416 (2008).

[7] G. Zhu, M. Schuricke, J. Steinmann, J. Albrecht, J. Ullrich, I. Ben-Itzhak, T. J. M. Zouros, J. Colgan, M. S. Pindzola, and A. Dorn, Phys. Rev. Lett. **103**, 103008 (2009).

[8] M. S. Pindzola and F. Robicheaux, Phys. Rev. A **57**, 318 (1998); **58**, 779 (1998).

[9] J. Colgan, M. S. Pindzola, and F. Robicheaux, J. Phys. B **34**, L457 (2001).

[10] M. S. Pindzola, F. Robicheaux, S. D. Loch, J. C. Berengut, T. Topcu, J. Colgan, M. Foster, D. C. Griffin, C. P. Ballance,

D. R. Schultz, T. Minami, N. R. Badnell, M. C. Witthoeft, D. R. Plante, D. M. Mitnik, J. A. Ludlow, and U. Kleiman, J. Phys. B **40**, R39 (2007).

[11] See http://physics.nist.gov/PhysRefData.

[12] J. Colgan and M. S. Pindzola, Phys. Rev. A **65**, 032729 (2002).

[13] J. A. R. Samson, W. C. Stolte, Z.-X. He, J. N. Cutler, Y. Lu, and R. J. Bartlett, Phys. Rev. A **57**, 1906 (1998).